Heliyon 6 (2020) e04493

Contents lists available at ScienceDirect

Heliyon

journal homepage: www.cell.com/heliyon

Research article

Green synthesis of antimicrobial silver nanoparticles using aqueous leaf extracts from three Congolese plant species (*Brillantaisia patula*, *Crossopteryx febrifuga* and *Senna siamea*)

Espoir K. Kambale [a], Christian I. Nkanga [a,b], Blaise-Pascal I. Mutonkole [a], Alain M. Bapolisi [b], Daniel O. Tassa [c], Jean-Marie I. Liesse [c], Rui W.M. Krause [b], Patrick B. Memvanga [a,*]

[a] *Laboratory of Pharmaceutics and Phytopharmaceutical Drug Development, Faculty of Pharmaceutical Sciences, University of Kinshasa, B.P. 212, Kinshasa XI, Democratic Republic of the Congo*

[b] *Center for Chemico- and Bio-Medicinal Research (CCBR), Department of Chemistry, Rhodes University, PO Box 94, Grahamstown 6140, Eastern Cape, South Africa*

[c] *Laboratory of Microbiology, Faculty of Pharmaceutical Sciences, University of Kinshasa, B.P. 212, Kinshasa XI, Democratic Republic of the Congo*

ARTICLE INFO

Keywords:
Green synthesis
Medicinal plants
Silver nanoparticles
Leaf aqueous extracts
Antibacterial activity
Engineering
Materials science
Chemistry
Biological sciences
Health sciences

ABSTRACT

In the present study, silver nanoparticles (AgNPs) were synthesized using aqueous leaf extracts of three Congolese plant species, namely *Brillantaisia patula* (BR-PA), *Crossopteryx febrifuga* (CR-FE) and *Senna siamea* (SE-SI). The obtained AgNPs were studied for their optical, structural, surface morphological and antibacterial properties. The prepared AgNPs were characterized by using UV-Visible spectra, Transmission Electron Microscopy (TEM), Fourier Transform Infrared Spectroscopy (FTIR), X-ray spectroscopy (EDX) and X-ray diffractometer (XRD). The synthesized nanoparticles were spherical shaped and well-dispersed with average sizes ranging from 45 to 110 nm. The AgNPs derived from BR-PA, CR-FE and SE-SI exhibited higher antibacterial activity against three bacterial pathogens of the human skin compared to their respective crude extracts and $AgNO_3$. This indicated that the biomolecules covering the nanoparticles may enhance the biological activity of metal nanoparticles. Hence, our results support that biogenic synthesis of AgNPs from Congolese plants constitutes a potential area of interest for the therapeutic management of microbial diseases such as infectious skin diseases.

1. Introduction

Used by mankind for about 7000 years, silver metal has been recognized as a very potent antibacterial agent, which is able to kill numerous types of microorganisms causing various infectious diseases (Chernousova and Epple, 2013). However, the application of silver metal on moisturized skin surface leads to low effective silver concentration since its oxidation to silver ions, which is required for the bactericidal activity, is a slow process under normal conditions (Griffith et al., 2015). To overcome this, silver salts were proposed as sources of ionic silver for the treatment of ulcers and burn wounds (Griffith et al., 2015). While the use of sparingly soluble silver salts (AgCl, AgBr, AgI and Ag_2S) leads to a slower release of silver ions (and lower antibacterial effects), the highly soluble $AgNO_3$ leads to high local silver concentration and deposition which damage the surrounding tissues (Chernousova and Epple, 2013). The clinical use of (ionic) silver is therefore limited due to its numerous adverse effects and high toxicity (argyria, allergic responses, leucopenia, bone marrow toxicity, renal or hepatic damage, etc.) (Burd et al., 2007; Poon and Burd, 2004).

Interestingly, when silver ions are transformed into metal silver nanoparticles (AgNPs) through biological and biomimetic methods of synthesis, their toxicity are seen to be reduced while their antimicrobial activities get enhanced markedly (Jadhav et al., 2016; Jain and Mehata, 2017; Liao et al., 2019; Singh et al., 2018). These characteristics make AgNPs wonderful weapons for the clinical management of microbial diseases (Liao et al., 2019), most specially as their selectivity towards bacterial cells have been proven and no case of antimicrobial resistance has been so far reported (Zhang et al., 2014). Indeed, AgNPs circumvent the ability of bacteria to mutate since one of their mechanisms of action is through destruction of the bacteria cells (Griffith et al., 2015; Zhang et al., 2014).

AgNPs are therefore emerging as high-value nanomaterials with unique features and extensive applications in various fields of

* Corresponding author.
E-mail address: patrick.memvanga@unikin.ac.cd (P.B. Memvanga).

https://doi.org/10.1016/j.heliyon.2020.e04493
Received 17 May 2020; Received in revised form 29 June 2020; Accepted 14 July 2020

pharmaceutical sciences, including the therapeutic management of infectious skin diseases (i.e. cellulitis, impetigo, acne, etc.) (Liao et al., 2019; Zhang et al., 2016). In the current development pipeline for new antibiotic medicines, AgNPs represent potent alternatives to the conventional antimicrobial treatment (de Jesús Ruíz-Baltazar et al., 2017). There are various antibacterial formulations and devices, like household antiseptic sprays, antimicrobial bandages, prosthetic implants and sutures, which have been designed and developed from AgNPs (Chernousova and Epple, 2013; Griffith et al., 2015; Zhang et al., 2016).

In comparison to the physical (high-energy irradiation, lithography, pyrolysis, laser ablation, mechanical milling, etc.) and chemical (microwave-assisted synthesis, electrochemical deposition, laser irradiation technique, photo-induced reduction, etc.) techniques used for the preparation of AgNPs, the biological synthesis pathways are eco-friendly, non-toxic, cost effective, simple and easily up-scalable for industrial production (Akhtar et al., 2013; Khan et al., 2018; Raji et al., 2019). Particularly, biological synthesis using plant extracts offers the advantages of producing nanoparticles with defined size and shape (Ethiraj et al., 2016), which are important features for various biomedical applications (Gurunathan et al., 2014; Liao et al., 2019). In fact, the intrinsic ability of plant metabolites to act as reducing and capping agents and contribute to amalgamation of metal ions into nanoparticles is more reputed than that of microorganisms (bacteria and fungi) (Makarov et al., 2014). Also, plant-mediated synthesis of AgNPs is much faster than the routes involving microorganism (Ahmed et al., 2016; Akhtar et al., 2013). Moreover, according to the "Traditional Medicine Strategy" proposed by the World Health Organization (2013), the use of green synthesis contributes to the valorisation of medicinal plants traditionally used in developing countries.

Of particular interest, plants with antimicrobial properties hold great potential for green synthesis of AgNPs against microbial diseases due to the complexity of their phytochemical composition (Khan et al., 2018; Makarov et al., 2014; Mishra et al., 2020; Rani et al., 2020). The most commonly found secondary metabolites include phenolics, flavonoids, tannins, alkaloids, terpenoids, etc., which mediate the green synthesis of AgNPs at molecular level thereby contributing to their antimicrobial activities (Kavitha et al., 2013; Khan et al., 2018; Makarov et al., 2014).

In this effect, the exploration of some indigenous plants for AgNPs synthesis represents a topic of current interest (Khan et al., 2018; Zhang et al., 2016). However, while the Democratic Republic of the Congo possesses a vast flora with an important biodiversity (>10000 species of plants), there is no report discussing the potential of Congolese medicinal plants for green synthesis of biofunctionalized AgNPs, to the best of our knowledge.

Therefore, the present study focused on the biosynthesis of AgNPs using the aqueous extracts from the leaves of *Brillantaisia patula* (BR-PA), *Crossopteryx febrifuga* (CR-FE) and *Senna siamea* (SE-SI). These species are used as antibacterial agents in the Congolese traditional medicine and, to the best of our knowledge and literature survey, they have not yet been used for the bio-production of AgNPs from silver ion solutions. Our investigation was therefore axed on physicochemical characterization of the biosynthesized nanoparticles using UV-Visible spectroscopy, transmission electron microscope (TEM), energy dispersive X-ray spectroscopy (EDX), X-ray diffraction (XRD) and Fourier transform infrared spectroscopy (FTIR). In addition, the antibacterial potentials of the greenly synthesized AgNPs were evaluated against some of the bacteria commonly involved in human diseases *viz.*, *Escherichia coli, Pseudomonas aeruginosa* and *Staphylococcus aureus*.

2. Materials and methods

2.1. Materials

The leaves of *Brillantaisia patula, Crossopteryx febrifuga* and *Senna siamea* were harvested in Matete Township (Kinshasa, DR Congo) in January 2019. Identity of plant materials was certified by Mr Nlandu Lukebiako at the *Institut National d'Etudes et des Recherches en Agronomie (INERA)* of the University of Kinshasa. Voucher specimens were handed in the herbarium of *INERA*, with voucher numbers P110899NL, P860342NL and P860343NL for *Brillantaisia patula*, *Crossopteryx febrifuga* and *Senna siamea*, respectively. The leaves were air-dried over one week at room temperature in the dark, and then ground to yield a fine powder. Silver nitrate (≥99.7 %) was purchased from Fisher Scientific (Leicestershire, UK). *Escherichia coli* ATCC25922, *Pseudomonas aeruginosa* ATCC27853, and *Staphylococcus aureus* ATCC25923 strains were sourced from the American Type Culture Collection (Manassas, VA, USA).

2.2. Methods

2.2.1. Preparation of leaf extracts and silver nanoparticles

2.2.1.1. Leaf extracts. Leaf powder (2.5 g) for each plant was boiled in 25 ml of distilled water for 15 min. The resultant extracts were subsequently filtered (90 mm filter discs, Boeco, Germany) and centrifuged at 4000 rpm for 20 min (MSE Mistral-1000 centrifuge, East Sussex, UK). The obtained leaf extracts were used as green reductants and capping agents for the biosynthesis of AgNPs.

2.2.1.2. AgNPs synthesis. A constant volume of 5 mM $AgNO_3$ (2 ml) was mixed with 2 ml, 4 ml or 8 ml of the leaf extracts. The final volumes were then adjusted to 10 ml by adding appropriate amounts of ultrapure water. The resultant mixtures were stirred at 300 rpm over 24 h at 70 °C. On cooling, the reaction media were centrifuged at 15000 rpm over 15 min (Beckman Coulter Allegra 64R, California, USA). The pellets were rinsed thrice with 10 ml of ultrapure water, freeze-dried, weighed and stored at room temperature in the dark for further characterizations. All the AgNPs batches were prepared in duplicate.

2.2.2. Physicochemical characterizations

Optical properties of the biosynthesized nanoparticles were investigated using UV–Visible spectroscopy. After diluting the samples with ultrapure water, the spectra were recorded as a function of wavelength on a Shimadzu UV-2550 spectrophotometer (Shimadzu, Kyoto, Japan) from 300 to 700 nm operated at a resolution of 1 nm. Ultrapure water was used as the blank for UV-Vis experiments (White et al., 2012; Jain and Mehata, 2017).

Particle morphology and shape were assessed using transmission electron microscopy (TEM) (Zeiss Libra-120 kV TEM microscope, Carl Zeiss, Oberkochen, Germany). For TEM experiment, the diluted samples were deposited dropwise onto carbon-coated copper TEM grids. The liquid in excess was absorbed using filter paper and the grids were allowed to air-dry overnight at room temperature prior to particle visualization. The software ImageJ-win32 was used to estimate the diameters of visualized nanoparticles (Bapolisi et al., 2020; Jain and Mehata, 2017; White et al., 2012). The mean diameters were estimated using log-normal fitting (Paramelle et al., 2014), a probability function commonly used for assessing skewed sizes distributions (DiPietro et al., 2010).

The crystallinity of the freeze-dried AgNPs was evaluated at room temperature by means of a X-ray diffractometer (XRD) (Bruker D8 Discover XRD, Berlin, Germany) using nickel filtered Cu Kα radiations set at 1.5404 Å, operating at 40 kV voltage and 30 mA current.

The biologically synthesized nanoparticles were placed on glass sample holders and the XRD patterns recorded in the range of 2θ from 10 to 100° with a scanning rate of 1°/min and a slit width of 6.0 mm (Nkanga et al., 2017). In order to assess the elemental surface composition of the biosynthesized AgNPs, the freeze-dried AgNP samples were drop-coated on to carbon film on an INCA PENTA FET connected to the VAGA TESCAM (Libusina, Czech Republic) for energy-dispersive X-ray spectroscopy (EDX). The EDX images were recorded at accelerating voltage of 20 kV (Singh et al., 2018). Fourier Transform Infrared (FT-IR) spectroscopic measurements were taken on a Perkin Elmer Spectrum 100 FT-IR Spectrophotometer (Massachusetts, USA) using attenuated total

reflection method. The FT-IR spectra were collected in the frequency range of 4000–650 cm^{-1} and 8 scans were done for each sample (Nkanga et al., 2017).

2.2.3. Antimicrobial activity evaluation

The assessment of antibacterial activity of AgNPs was carried out by using three different test pathogens namely *Staphylococcus aureus* (gram-positive), *Escherichia coli* and *Pseudomonas aeruginosa* (gram-negative).

A standard broth microdilution method was used to determine the minimal inhibitory concentrations (MIC) of AgNPs *viz.*, the lowest concentration that can completely inhibit the visible growth of microorganisms after incubating overnight (Jain and Mehata, 2017). Based on the study by Olivier et al. (2018), which reported a MIC of 500 μg/ml, the concentrations investigated in this work ranged from 1200 to 18.75 μg/ml, 20000–156.25 μg/ml and 8500–531.25 μg/ml for AgNPs, leaf extracts and $AgNO_3$, respectively. Briefly, serial two-fold dilutions of AgNPs leaf extracts and $AgNO_3$ in Mueller-Hinton Broth were prepared in sterile microtubes using distilled water as solvent. The 24 h-cultures of microbial strains were stirred with 0.9 % NaCl to achieve 0.5 Mc Farland standard (approximately 10^8 colony forming units (cfu)/ml). Thereafter, 1 ml of the final inocula adjusted to 10^6 cfu/ml was supplemented with equal volumes of each sample test (AgNPs, extracts and $AgNO_3$). The obtained mixtures were incubated at 37 °C for 24 h in ambient atmosphere. Finally, the microtubes were visually examined for turbidity, with cloudiness indicating that bacterial growth was not inhibited by the concentration of sample tests contained in the medium (Jain and Mehata, 2017).

3. Results and discussion

3.1. Formation of AgNPs

3.1.1. Observation of color change and UV-Vis spectroscopy

The successful synthesis of AgNPs using the investigated Congolese plant extracts were confirmed by color change and spectroscopic analysis of the reaction medium and isolated nanoparticles. Indeed, after stirring the mixture of $AgNO_3$ and plant extracts for 10 min, an obvious color change was observed for all the three plants studied. The color of the reaction mixture changed from yellowish green to brown, suggesting the conversion of ionic silver (Ag^+) to metallic silver (Ag°) that self-ensembles into colloidal particles (AgNPs). This observation is consistent with the established literature (Oliveira et al., 2019; Singh et al., 2018), which stipulates that silver ions are reduced in the presence of plant extracts due to the reducing properties of some secondary metabolites (i.e. polyphenols, alkaloids, terpenoids, proteins, etc.) (Gurunathan et al., 2014; Jadhav et al., 2016; Jain and Mehata, 2017).

In fact, the brown color of AgNPs arises from the concomitant vibration of free electrons of the metallic silver that are in resonance with the light wave. This explains the origin of the surface plasmon resonance (SPR) absorption often observed with metallic nanoparticles, which is commonly verified using UV-Vis spectroscopy to complement the visual observation (colour change) in establishing AgNPs formation. As shown in Figure 1, all the synthesized AgNPs exhibited distinctive UV-Vis absorption bands with maximum absorbances at 434 nm, 522 nm and 489 nm for the nanoparticles from BR-PA, SE-SI and CR-FE, respectively. The observed UV-Vis bands are due to the SPR absorption and confirm the presence of AgNPs, alike the color change. Surprisingly, there were remarkable differences in the maximum absorption wavelengths between the AgNPs from the three plants. This could be due to the fact that the synthesized AgNPs are interacting with phytoconstituents of different origins, leading to variable interferences with the SPR absorption signatures. Nonetheless, the molecular and surface analysis of the biosynthesized AgNPs (EDX, FT-IR) were further supportive in verifying and establishing the presence of organic phytochemicals in the produced nanomaterials.

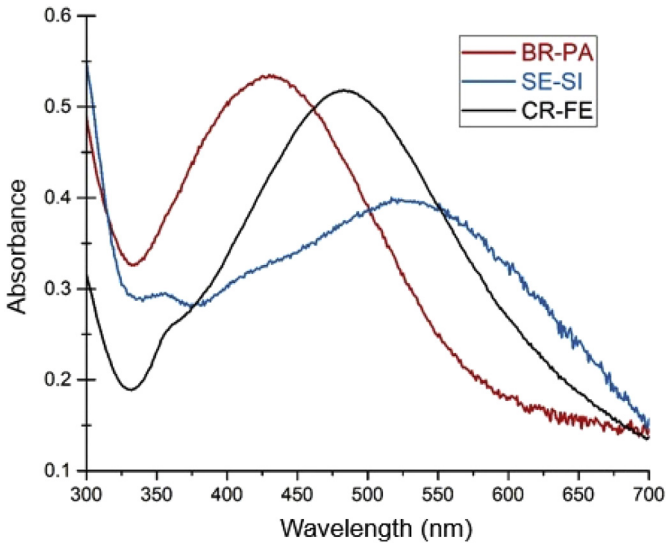

Figure 1. UV-Vis absorption spectra of AgNPs synthesized using BR-PA, SE-SI and CR-FE.

3.1.2. Analysis of TEM images

The microscopic observation of the bio-synthetic reaction medium allowed verifying the formation of colloidal particles (AgNPs). Figure 2 presents typical TEM images of the biosynthesized nanomaterials. These illustrative micrographs show the presence of individual nanoparticles with almost spherical shape and roughly no particle aggregates, which is characteristic to AgNPs (Chaudhari et al., 2012). The particle sizes (and size distribution) of the synthesized AgNPs were estimated under TEM visualization using ImageJ software, and were found to be about 45 nm (with polydispersity of 32.1%), 115 nm (with polydispersity of 10.8%) and 47 nm (with polydispersity of 46.0%), respectively for the particles from BR-PA, SE-SI and CR-FE. This confirms the nanoparticulate nature of the synthesized materials and supports the observation from the UV-Vis spectroscopy, regarding the successful formation of colloidal particles from silver ions in the presence of aqueous leaf extracts of the Congolese plants. In addition, all the ImageJ graphs described a Gaussian distribution peak at around the average sizes estimated for each nanoparticle formulation (Figure 2), which shows acceptable particle size distribution as observed with polydispersity values below 50%.

3.2. AgNPs surface analysis

3.2.1. EDX

The assessment of the elemental composition on the surface of the biosynthesized nanomaterials was done using EDX spectroscopy. In general, the optical absorption peak of silver appears at around 3 keV due to the SPR (Magudapatty et al., 2001; Singh et al., 2018). As shown in Figure 3, EDX analysis revealed the presence of silver in the nanoparticles formulated from all the three Congolese species. While silver peaks were the most prominent for all the samples, the EDX patterns of the prepared formulations did not exhibit any nitrogen peaks. This indicates the absence of noticeable traces of ions from $AgNO_3$ initially used, which confirms the presence of metallic silver in the sample and evidences of successful reduction of silver ions as suggested by visual observation and UV-Vis spectroscopy (see Figure 1).

In addition to silver peaks, EDX unveiled the presence of carbon and oxygen atoms in the nanoparticle samples (Figure 3). This suggests the existence of organic compounds (phytochemicals) on the surface of the biosynthesized AgNPs, supporting the fact that AgNPs from the three plants did not exhibit similar SPR absorption bands on UV-Vis spectroscopy. Since plant secondary metabolites act not only as reducing agents but also as capping agents for AgNPs (Bagur et al., 2019; Makarov et al.,

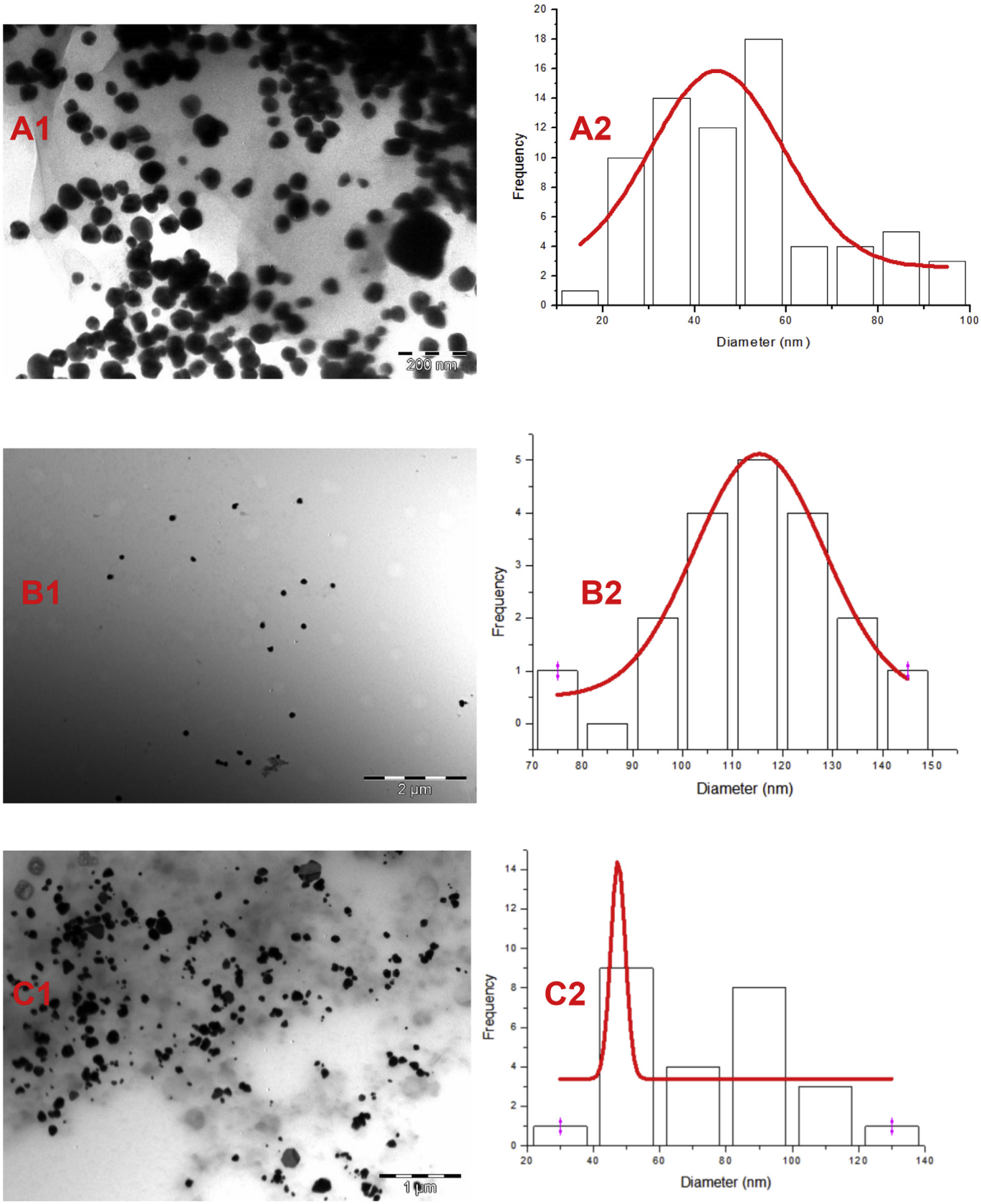

Figure 2. AgNPs shape and size distribution: TEM micrographs and ImageJ graphs of AgNPs obtained using BR-PA (A1 and A2), SE-SI (B1 and B2) and CR-FE (C1 and C2). The curves on ImageJ graphs describe the log-normal fitting to the estimated physical diameters (represented by histograms). The mean diameters derived from the log-normal function.

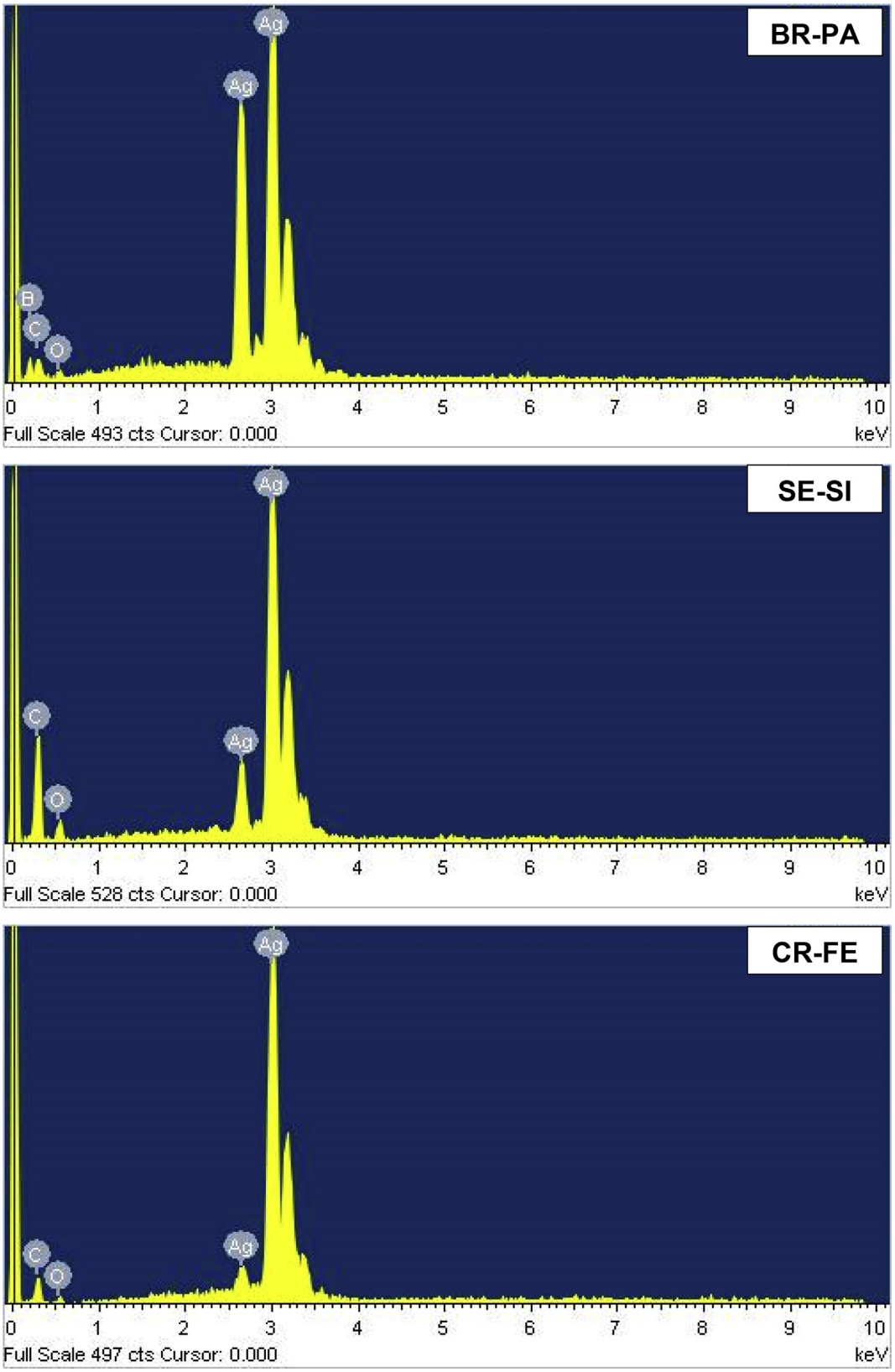

Figure 3. EDX spectra of green synthesized AgNPs using BR-PA, SE-SI and CR-FE.

2014), the difference in the phytochemical composition of the three plants could be the reason for the observed variabilities in the UV-Vis absorption and nano-sizes of the biosynthesized AgNPs (as the AgNPs are capped by different leaf extract biomolecules, being from different plants).

3.2.2. FTIR

The FTIR spectroscopic analysis aimed at verifying the chemical composition of the nanoparticles surface, confirming the formation and capping of AgNPs, and comparing the molecular profiles of the three batches of nanomaterials synthesized from different plants.

Figure 4 presents the FTIR spectra of the nanoparticles synthesized using BR-PA, SE-SI and CR-FE. From all the spectra recorded, several stretching vibration bands related to organic functional groups were prominently observed. These include the presence of round-shaped bands at around 3325–3198 cm^{-1}, 2917–2833 cm^{-1}, 1380–1360 cm^{-1}, and 1050–1025 cm^{-1}, which correspond to the vibrations of alcoholic O–H, alkanes C–H, phenolic O–H and C–O stretches, respectively (Gomathi et al., 2017; Jain and Mehata, 2017; Singh et al., 2018). Moreover, the stretching mode of carbonyl group (C=O) was observed at 1640–1620 cm^{-1}, suggesting the presence of carboxylic, aldehydes, esters or ketone containing compounds (Ajitha et al., 2015; Rónavári et al., 2017). The outcome from FTIR analysis is consistent with EDX data regarding the existence of carbon and oxygen on the surface of AgNPs, since it indicates the presence of organic compounds (phytoconstituents) in the nanoparticle samples, as reported by Kumari et al. (2020).

Most importantly, the FTIR spectra of the synthesized nanoparticles did not exhibit a stretching band related to the nitro bond (N–O) at around 1280 cm^{-1}, indicating the absence of noticeable traces of nitrates (Bagur et al., 2019), which agrees with our EDX data (where N was not observed). This confirms successful formation of AgNPs thanks to the phytomolecules (secondary metabolites) that may act as both reducing and capping agents. FTIR results lend support to our UV-Vis spectroscopy analysis regarding the molecular interactions between the synthesized nanoparticles and phytochemicals, which led to variations in the SPR absorption and particle sizes of AgNPs from the three plants. Moreover, the produced AgNPs batches exhibited FTIR molecular profiles with different vibration bands (Figure 4), since they are expected to bear different types of secondary metabolites on the surface as they derived from different plants. In order to confirm these discrepancies between the three batches prepared, the crystallinity of the biosynthesized AgNPs was investigated.

3.3. Crystallinity of AgNPs

The crystallinity of the biosynthesized nanoparticles was evaluated using XRD. The XRD patterns presented in Figure 5 show several Braggs reflections with various 2θ values depending on the AgNPs batches. Nevertheless, all the three AgNP formulations exhibited four diffraction peaks (marked with asterisks in Figure 5), at 2θ = 38.19°, 44.24°, 64.54° and 77.36°, which correspond to the reflection of (111), (200), (220), and (311) planes of face-centered cubic lattice structure of metallic silver (JCPDS-ICDD files No 04-0783). This confirms successful synthesis of AgNPs and establishes their crystalline nature (Dhand et al., 2016; Rónavári et al., 2017). Similar diffraction patterns were observed with

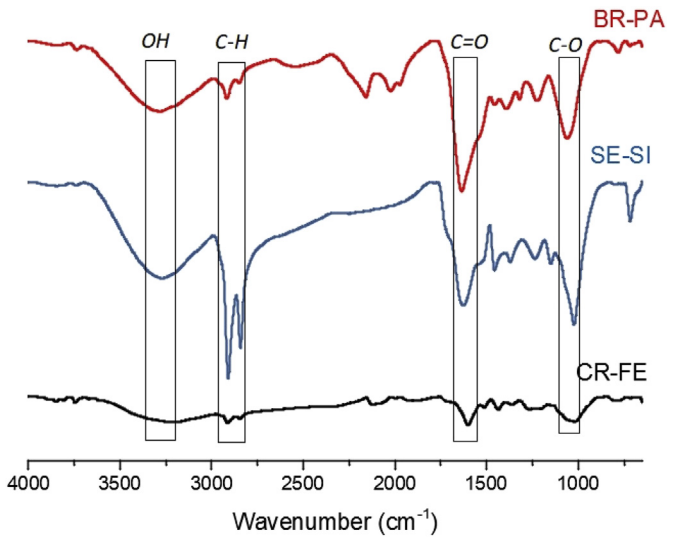

Figure 4. FTIR spectra of the bio-reduced AgNPs using BR-PA, SE-SI and CR-FE.

AgNPs greenly synthesized using other plant extracts (Ajitha et al., 2015; Jain and Mehata, 2017; Oliveira et al., 2019).

Noteworthy, these four characteristic peaks are the maximum one should expect for highly pure AgNPs (Anthony et al., 2014). Concerning our synthesized nanomaterials, additional peaks were observed in the XRD patterns (at 2θ = 27.87°, 32.32°, 46.31° and 54.88°) thereby indicating that our synthesized nanomaterials did not contain silver metal 100% but were mixed with other substances (phytochemical/capping agents). Indeed, the XRD profiles confirm the presence of organic compounds in the sample, since the Braggs reflection appearing between 2θ = 24.48° and 32.50° are often assigned to the crystalline and amorphous organic phases (Gurunathan et al., 2014). These data agree with those of from the FTIR, EDX and UV-Vis spectroscopy. Moreover, as framed by the dashed greys in Figure 5, AgNPs from the three plants show distinctive variability in XRD peaks intensity and position. This shows the difference in the crystallinity of the investigated products, and clearly demonstrates the difference in the chemical composition of the AgNPs batches, which stands to the reason since the extracts yielded different capping agents (being from different plants).

3.4. Antibacterial activity of AgNPs

Antibacterial effects of AgNPs were investigated against *E. coli, P. aeruginosa* and *S. aureus* through determination of the MICs. As presented in Table 1, BR-PA showed MICs greater than 10000 μg/ml, which indicate poor activity against the tested bacterial strains compared with the MICs of SE-SI and CR-FE. These results corroborate with those obtained by Faparusi et al. (2012) and Fomogne-Fodjo et al. (2014). However, the AgNPs from BR-PA exhibited remarkable antibacterial activities, which were found to be greater than those of AgNPs from SE-SI and CR-FE (Table 1). This could be explained by the fact that very specific phytoactive compounds covered the AgNPs from BR-PA (see the 2500-1750 cm^{-1} region of the FTIR spectra, Figure 4). These phytochemicals that may act as reducing and/or capping agents would preferentially involve in the reduction of Ag^{+} ions into Ag° metal and in the phytochemical-assisted fabrication of AgNPs from BR-PA (nucleation, capping and stabilization) (Akhtar et al., 2013; Makarov et al., 2014; Rónavári et al., 2017).

Moreover, these botanic compounds may have inherent strong antibacterial activities which would unfortunately be diluted in the crude extract due to their presence in small amounts. Indeed, literature reported that many phytochemicals (polyphenols, alkaloids, terpenoids, etc.) exhibit antimicrobial properties (Othman et al., 2019; Raji et al., 2019). Additional studies including bio-guided fractionation, high performance liquid chromatography-mass spectrometry (HPLC-MS) and nuclear magnetic resonance (NMR)analyses would be useful to determinate the class of the phytoconstituent compounds located on the AgNPs surface and acting as capping agents, as well as to elucidate their chemical structure (White et al., 2012).

The bactericidal effects of AgNPs also depend on the nanoparticle characteristics, including the size and the shape (Liao et al., 2019; Rónavári et al., 2017). Indeed, the size of AgNP BR-PA (45 nm, Figure 2) is 2-fold smaller than of AgNP from SE-SI, which might have increased their surface area, promoted bacterial cell wall interactions and membrane permeability and therefore enhanced their antibacterial activity by leakage of cellular contents. After penetrating in the cytoplasm of bacteria, silver nanoparticles can also disturb the cell function by interacting with amino acids and enzymes, causing generation of reactive oxygen species (ROS) and destruction of bacterial deoxyribonucleic acid (DNA) (Liao et al., 2019; Rónavári et al., 2017).

Moreover, in aerobic conditions, silver metals from AgNPs dispersed in aqueous solutions can be chemically oxidized to release silver ions which are also responsible for antibacterial activity (Chernousova and Epple, 2013; Liao et al., 2019). Due to their higher surface-to-volume ratio, small AgNPs from BR-PA can release more Ag^{+} ions than large AgNPs from SE-SI (Liao et al., 2019; Rónavári et al., 2017). Indeed, the

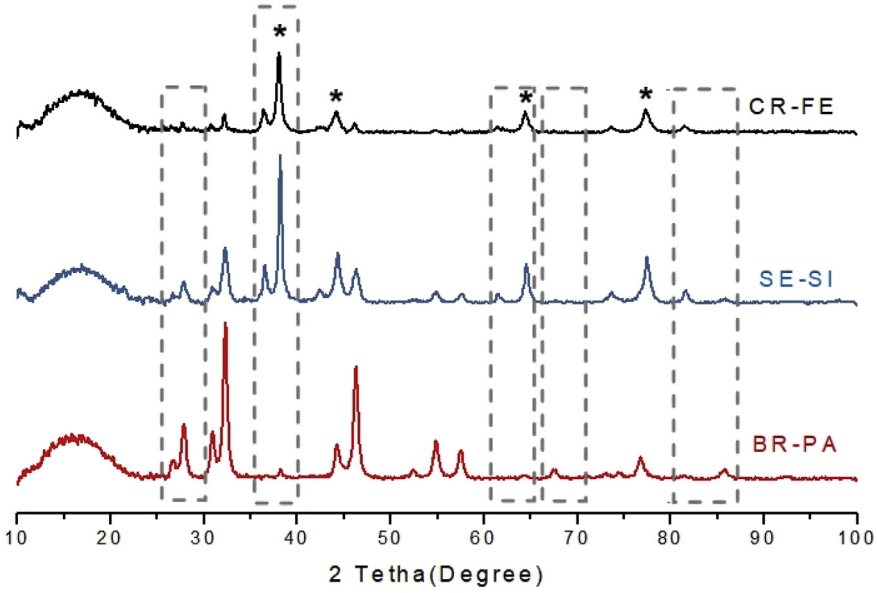

Figure 5. XRD spectra of AgNPs synthesized using BR-PA, SE-SI and CR-FE. Dashed grey frames show peak differences between the three diffractograms, while asterisks (*) indicate common peaks that are characteristics to AgNPs.

Table 1. Minimum inhibitory concentration (MIC) of the greenly synthesized AgNPs.

	MIC (μg/ml)		
	E. coli	*P. aeruginosa*	*S. aureus*
AgNPs from BR-PA	<9.375	18.75	75
AgNPs from CR-FE	150	75	300
AgNPs from SE-SI	75	150	37.5
BR-PA	>10000	>10000	>10000
CR-FE	2500	1250	2500
SE-SI	5000	1250	312.5
$AgNO_3$	<265.625	<265.625	531.25

more silver ions are released the greater will be the AgNPs-induced cellular toxicity (Rónavári et al., 2017).

Concerning CR-FE, the results indicate that its aqueous extract has MICs between 1250 and 2500 μg/ml (Table 1), which is consistent with previous results (Chouna et al., 2015; Halilu et al., 2012). These MICs are 2 times higher with *E. coli* and *S. aureus* (MIC = 2500 μg/ml) than with *P. aeruginosa* (MIC = 1250 μg/ml). As for the AgNPs synthesized using CR-PE, the same trend was observed between *E. coli* (MIC = 150 μg/ml) and *P. aeruginosa* (MIC = 75 μg/ml). However, with *S. aureus* (MIC = 300 μg/ml), the trend is reversed and the MIC appeared 4 times higher than that of *P. aeruginosa*. The difference in the structural composition of capping agents that form layer covering both AgNPs synthesized using CR-FE and BR-PA may explain the discrepancy observed in their biological activity, independently of their similar size (Rónavári et al., 2017).

Based on all these results, we concluded that silver nanoparticles greenly fabricated in our study showed much greater anti-microbial activity than the plant extracts, which lend support to the data previously reported (Rónavári et al., 2017). Noteworthy, the AgNPs synthesized using BR-PA and CR-FE were found to be more active against the tested gram-negative bacteria (*E. coli* and *P. aeruginosa*) than the gram-positive bacteria (*S. aureus*). This is in line with previous reports (Bala et al., 2015; Liao et al., 2019) suggesting that gram-negative bacteria are generally more prone to Ag^+ invasion than gram-positive bacteria due to the difference in their cell wall structures. Indeed, gram-negative bacteria possess a single peptidoglycan layer, thus Ag^+ ions can easily damage the cell wall. However, gram-positive bacteria have a very thick cell wall containing many peptidoglycan layers, thereby serving as a barrier for Ag^+ ions penetration into the cytoplasm (Liao et al., 2019). Importantly, it should be noted that contrary results have been obtained with AgNP from SE-SI. This could be explained by the fact that, at the outset, the extract already appeared to be 15 times more active against *S. aureus* than *E. coli* and *P. aeruginosa*, as previously reported (Nas et al., 2018).

4. Conclusion

The present study demonstrated the eco-friendly, inexpensive, facile and fast synthesis of AgNPs using aqueous leaf extracts of Congolese plant species frequently used in traditional medicine, namely *Brillantaisia patula*, *Crossopteryx febrifuga* and *Senna siamea*. Various physico-chemical characterization techniques confirmed successful formation of spherical and crystalline AgNPs and evidenced the role of phytochemicals from the extracts as reducing and capping agents in the green synthesis of AgNPs. Moreover, the biological evaluation of AgNPs revealed good bactericidal properties against *Staphylococcus aureus*, *Escherichia coli*, and *Pseudomonas aeruginosa*, which are pathogens commonly involved in infectious skin diseases. Hence, this study testifies that bio-functionalized AgNPs obtained by green synthesis using medicinal plants hold the potential to tackle microbial cutaneous disorders (i.e. *Staphylococcus* and *Pseudomonas* infections, ulcers, burn wounds, etc.) and antibiotic resistance. Nevertheless, our labs have launched several studies addressing the formulation of AgNPs-based topical dosage forms for further cost-effective phytomedicines development.

Declarations

Author contribution statement

E.K. Kambale: Conceived and designed the experiments; Performed the experiments; Analyzed and interpreted the data.

C.I. Nkanga: Performed the experiments; Analyzed and interpreted the data; Wrote the paper.

B.P.I. Mutonkole and A.M. Bapolisi: Performed the experiments; Analyzed and interpreted the data.

D.O. Tassa: Conceived and designed the experiments; Performed the experiments.

J.M.I. Liesse: Conceived and designed the experiments; Contributed reagents, materials, analysis tools or data.

R.W.M. Krause: Analyzed and interpreted the data; Contributed reagents, materials, analysis tools or data; Wrote the paper.

P.B. Memvanga: Conceived and designed the experiments; Analyzed and interpreted the data; Contributed reagents, materials, analysis tools or data; Wrote the paper.

Funding statement

This work was partially supported by the National Research Foundation of South Africa and the Sandisa Imbewu Programme of Rhodes University (South Africa).

Competing interest statement

The authors declare no conflict of interest.

Additional information

No additional information is available for this paper.

Acknowledgements

Dr Christian I. Nkanga and Mr Alain M. Bapolisi are thankful to the NGO *Förderverein Uni Kinshasa e. V., fUNIKIN, Else-Kroener-Fresenius Stiftung* and *Holger-Poehlmann* Foundation for their support through the Excellence Scholarship Program BEBUC (*Bourse d'Excellence Bringmann aux Universités Congolaises*).

References

Ahmed, S., Ahmad, M., Swami, B.L., Ikram, S., 2016. A Review on Plants extract mediated synthesis of silver nanoparticles for antimicrobial applications: a green expertise. J. Adv. Res. 7, 17–28.

Ajitha, B., Reddy, Y.A.K., Shameer, S., Rajesh, K.M., Suneetha, Y., Reddy, P.S., 2015. *Lantana camara* leaf extract mediated silver nanoparticles: antibacterial, green catalyst. J. Photochem. Photobiol., B 149, 84–92.

Akhtar, M.S., Panwar, J., Yun, Y.S., 2013. Biogenic synthesis of metallic nanoparticles by plant extracts. ACS Sustain. Chem. Eng. 1, 591–602.

Anthony, K.J.P., Murugan, M., Jeyaraj, M., Rathinam, N.K., Sangiliyandi, G., 2014. Synthesis of silver nanoparticles using pine mushroom extract: a potential antimicrobial agent against *E. coli* and *B. subtilis*. J. Ind. Eng. Chem. 20, 2325–2331.

Bagur, H., Poojari, C.C., Melappa, G., Rangappa, R., Chandrasekhar, N., Somu, P., 2019. Biogenically synthesized silver nanoparticles using endophyte fungal extract of *Ocimum tenuiflorum* and evaluation of biomedical properties. J. Cluster Sci. 1–15.

Bala, N., Saha, S., Chakraborty, M., Maiti, M., Das, S., Basub, R., Nandyc, P., 2015. Green synthesis of zinc oxide nanoparticles using *Hibiscus subdariffa* leaf extract: effect of temperature on synthesis, anti-bacterial activity and anti-diabetic activity. RSC Adv. 5, 4993–5003.

Bapolisi, A.M., Nkanga, C.I., Walker, R.B., Krause, R.W.M., 2020. Simultaneous liposomal encapsulation of antibiotics and proteins: Co-loading and characterization of rifampicin and Human Serum Albumin in soy-liposomes. J. Drug Deliv. Sci. Technol. 58, 1–12.

Burd, A., Kwok, C.H., Hung, S.C., Chan, H.S., Gu, H., Lam, W.K., Huang, L., 2007. A comparative study of the cytotoxicity of silver-based dressings in monolayer cell, tissue explant, and animal models. Wound Repair Regen. 15, 94–104.

Chaudhari, P.R., Masurkar, S.A., Shidore, V.B., Kamble, S.P., 2012. Effect of biosynthesized silver nanoparticles on *Staphylococcus aureus* biofilm quenching and prevention of biofilm formation. Nano-Micro Lett. 4, 34–39.

Chernousova, S., Epple, M., 2013. Silver as antibacterial agent; ion, nanoparticle, and metal. Angew. Chem. Int. Ed. 52, 1636–1653.

Chouna, J.R., Tamokou, J.D., Nkeng-Efouet-Alango, P., Lenta, B.N., Sewald, N., 2015. Antimicrobial triterpenes from the stem bark of *Crossopteryx febrifuga*. Z Naturforsch. C. J. Biosci. 70, 169–173.

De Jesús Ruíz-Baltazar, A., Yobbany, S.R.L., Larrañaga, D., Pérez, R., 2017. Green synthesis of silver nanoparticles using a *Melissa officinalis* leaf extract with antibacterial properties. Results in Phys 7, 2639–2643.

Dhand, V., Soumya, L., Bharadwaj, S., Chakra, S., Bhatt, D., Sreedhar, B., 2016. Green synthesis of silver nanoparticles using *Coffea arabica* seed extract and its antibacterial activity. Mater Sci. Eng. C. Mater. Biol. Appl. 58, 36–43.

DiPietro, R.S., Johnson, H.G., Bennett, S.P., Nummy, T.J., Lewis, L.H., Heiman, D., 2010. Determining magnetic nanoparticle size distributions from thermomagnetic measurements. Appl. Phys. Lett. 96, 222506.

Ethiraj, A.S., Jayanthi, S., Ramalingam, C., Banerjee, C., 2016. Control of size and antimicrobial activity of green synthesized silver nanoparticles. J. Mater. Lett. 185, 526–529.

Faparusi, F., Belo-Akinosho, M., Oyede, R., Adewole, A., Bankole, P., Ali, F., 2012. Phytochemical screening and antibacterial activity of *Brillantaisia patula* leaf. Res. J. Phytochem. 6, 9–16.

Fomogne-Fodjo, M.C.Y., Van Vuuren, S., Ndinteh, D.T., Krause, R.W.M., Olivier, D.K., 2014. Antibacterial activities of plants from Central Africa used traditionally by the Bakola pygmies for treating respiratory and tuberculosis-related symptoms. J. Ethnopharmacol. 155, 123–131.

Gomathi, M., Rajkumar, P.V., Prakasam, A., Ravichandran, K., 2017. Green synthesis of silver nanoparticles using *Datura stramonium* leaf extract and assessment of their antibacterial activity. Resour. Eff. Technol. 3, 280–284.

Griffith, M., Udekwu, K.I., Gkotzis, S., Mah, T.F., Alarcon, E.I., 2015. "Anti-microbiological and anti-infective activities of silver," *in silver nanoparticle applications*. In: Alarcon, I.E., Griffith, M., Udekwu, I.K. (Eds.), The Fabrication and Design of Medical and Biosensing Devices. Springer International Publishing, Cham, pp. 127–146.

Gurunathan, S., Han, J.W., Kwon, D., Kim, J.H., 2014. Enhanced antibacterial and anti-biofilm activities of silver nanoparticles against gram-negative and gram-positive bacteria. Nanoscale Res. Lett. 9, 373.

Halilu, M.E., Abubakar, A., Garba, M.K., Isah, A.A., 2012. Antimicrobial and preliminary phytochemical studies of methanol extract of root bark of *Crossopteryx febrifuga* (Rubiaceae). J. Appl. Pharmaceut. Sci. 2, 66–70.

Jadhav, K., Dhamecha, D., Bhattacharya, D., Patil, M., 2016. Green and ecofriendly synthesis of silver nanoparticles: characterization, biocompatibility studies and gel formulation for treatment of infections in burns. J. Photochem. Photobiol., B 155, 109–115.

Jain, S., Mehata, M.S., 2017. Medicinal plant leaf extract and pure flavonoid mediated green synthesis of silver nanoparticles and their enhanced antibacterial property. Sci. Rep. 7, 1–13.

Kavitha, K.S., Baker, S., Rakshith, D., Kavitha, H.U., Rao, Y.H.C., Harini, B.P., Satish, S., 2013. Plants as green source towards synthesis of nanoparticles. Int. Res. J. Biol. Sci. 2, 66–76.

Khan, S.U., Saleh, T.A., Wahab, A., Khan, M.H.U., Khan, D., Khan, W.U., Rahim, A., Kamal, S., Khan, F.U., Fahad, S., 2018. Nanosilver: new ageless and versatile biomedical therapeutic scaffold. Int. J. Nanomed. 13, 733–762.

Kumari, R., Mishra, R.C., Yadav, J.P., 2020. Antioxidant and cytotoxic studies of *Acacia nilotica* twig extract and their green synthesized silver nanoparticles. Lett. Appl. Nanobiosci. 9, 975–980.

Liao, C., Li, Y., Tjong, S.C., 2019. Bactericidal and cytotoxic properties of silver nanoparticles. Int. J. Mol. Sci. 20, 449.

Magudapatty, P., Gangopadhyayrans, P., Panigrahi, B.K., Nair, K.G.M., Dhara, S., 2001. Electrical transport studies of Ag nanoparticles embedded in glass matrix. Physica B 299, 142–146.

Makarov, V.V., Love, A.J., Sinitsyna, O.V., Makarova, S.S., Yaminsky, I.V., Taliansky, M.E., Kalinina, N.O., 2014. Green nanotechnologies: synthesis of metal nanoparticles using plants. Acta Naturae 6, 35–44.

Mishra, R.C., Kumari, R., Iqbal, Z., Rizvi, M.A., Yadav, J.P., 2020. Synthesis, characterization, comparative antidandruff efficacy and cytotoxicity studies of biosynthesized silver nanoparticles by using *Glycyrrhiza glabra* root. Adv. Sci. Eng. Med. 12, 156–162.

Nas, F.S., Oyeyi, T.I., Ali, M., 2018. Antibacterial efficacy and phytochemical screening of *Senna siamea* leaves extracts on some pathogenic bacteria. J. Microbiol. Exp. 6, 159–163.

Nkanga, C.I., Krause, R.W., Noundou, X.S., Walker, R.B., 2017. Preparation and characterization of isoniazid-loaded crude soybean lecithin liposomes. Int. J. Pharm. 526, 466–473.

Oliveira, G.Z.S., Lopes, C.A.P., Sousa, M.H., Silva, L.P., 2019. Synthesis of silver nanoparticles using aqueous extracts of *Pterodon emarginatus* leaves collected in the summer and winter seasons. Int. Nano Lett. 9, 109–117.

Olivier, N.E., Oscar, N.D.Y., Alima, N.L.N., François, M.G., Barthelemy, N., 2018. Antibacterial properties of the extracts of *Allexis obanensis* and *Allexis batangae* (Violaceae) collected at Kribi (South Cameroon). J. Phytol. 7, 275–284.

Othman, L., Sleiman, A., Abdel-Massih, M., 2019. Antimicrobial activity of polyphenols and alkaloids in Middle Eastern plants. Front. Microbiol. 10, 911.

Paramelle, D., Sadovoy, A., Gorelik, S., Free, P., Hobleya, J., Fernig, D.G., 2014. A rapid method to estimate the concentration of citrate capped silver nanoparticles from UV-visible light spectra. Analyst 139, 4855–4861.

Poon, V.K.M., Burd, A., 2004. *In vitro* cytotoxicity of silver: implication for clinical wound care. Burns 30, 140–147.

Raji, P., Samrot, A.V., Keerthana, D., Karishma, S., 2019. Antibacterial activity of alkaloids, flavonoids, saponins and tannins mediated green synthesized silver. J. Cluster Sci. 30, 881–885.

Rani, R., Sharma, D., Chaturvedi, M., Yadav, J.P., 2020. Green synthesis of silver nanoparticles using *Tridax procumbens*: their characterization, antioxidant and antibacterial activity against MDR and reference bacterial strains. Chem. Pap. 74, 1817–1830.

Rónavári, A., Kovács, D., Igaz, N., Vágvölgyi, C., Boros, I.M., Kónya, Z., Pfeiffer, I., Kiricsi, M., 2017. Biological activity of green-synthesized silver nanoparticles depends on the applied natural extracts: a comprehensive study. Int. J. Nanomed. 12, 871–883.

Singh, H., Du, J., Singh, P., Yi, T.H., 2018. Ecofriendly synthesis of silver and gold nanoparticles by *Euphrasia officinalis* leaf extract and its biomedical applications. Artif. Cells Nanomed. Biotechnol. 46, 1163–1170.

White 2nd, G.V., Kerscher, P., Brown, R.M., Morella, J.D., McAllister, W., Dean, D., Kitchens, C.L., 2012. Green synthesis of robust, biocompatible silver nanoparticles using garlic extract. J. Nanomater. 2012, 730746.

WHO Press, Geneva, 2013. Traditional Medicine Strategy 2014-2023.

Zhang, C., Liang, Z., Hu, Z., 2014. Bacterial response to a continuous long-term exposure of silver nanoparticles at sub-ppm silver concentrations in a membrane bioreactor activated sludge system. Water Res. 50, 350–358.

Zhang, X.F., Liu, Z.G., Shen, W., Gurunathan, S., 2016. Silver nanoparticles: synthesis, characterization, properties, applications, and therapeutic approaches. Int. J. Mol. Sci. 17, 1534.